ORIGINAL ARTICLE

Optimizing the gasification performance of biomass chemical looping gasification: enhancing syngas quality and tar reduction through red mud oxygen carrier

Zhonghui Wang[1] · Long Han[1,2] · Zewei Shen[1] · Kaili Ma[1] · Yuelun Wu[1] · Jianhao Zhang[1] · Shengxiao Mao[1]

Abstract

Biomass chemical looping gasification (BCLG) is a promising technology for producing high-quality syngas. In this study, the BCLG of corn cob using inexpensive industrial waste red mud (RM) as an oxygen carrier was carried out in a fixed bed reactor, focusing on enhancing syngas quality and tar reduction. The gasification performance of BCLG was investigated under different conditions, including O/C ratio, steam flow rate, and reaction temperature. RM improved gas yield and quality with a maximum H_2/CO ratio of 2.39 while reducing tar yield by 38.75%. High temperature led to the polymerization of polyaromatic hydrocarbons (PAHs) in tar, but steam effectively reduced PAHs by 33.25% via the tar homogeneous conversion. The degree of tar cracking and conversion to gases in the presence of steam was more than the thermal decomposition in the pure N_2 atmosphere. Additionally, metal oxides within RM participated in reactions with steam. The limitation of intensive reduction of RM through iron-steam reactions enhanced H_2 yield and prevented RM sintering. XRD analyses revealed the evolution of iron compounds in RM during BCLG: Fe_2O_3—Fe_3O_4—FeO/Fe—Fe_3O_4. Under the optimal conditions of BCLG, the carbon conversion efficiency, gasification efficiency, and gas yield reached 70.74%, 92.95%, and 1.24 m^3/kg, respectively. Meanwhile, the H_2/CO ratio reached 1.82 while the tar yield was reduced to 0.196 g/g_{fuel}. This study highlighted the potential of using RM as an effective oxygen carrier in the BCLG, which would contribute to the advancement of sustainable biomass gasification.

Keywords Chemical looping gasification · Red mud · Hydrogen production · Tar cracking · Biomass

1 Introduction

The global energy demand is undergoing a substantial transformation, characterized by a transition from fossil fuels to clean and renewable energy sources [1]. The development and utilization of biomass energy are of great significance from the point of view of alleviating the global energy shortage and protecting the environment. Biomass chemical looping gasification (BCLG) is a novel clean technology for converting biomass into high-quality combustible gas

[2, 3]. The BCLG process utilizes a metal oxygen carrier as a substitute for pure oxygen to facilitate the oxidation and reduction between the fuel reactor and air reactor, which enables the transfer of lattice oxygen and heat [4, 5]. However, the feasibility of the BCLG technology faces two major challenges: the expensive cost of oxygen carriers [6–9] and the disposal of excessive tar [10–12].

Red mud (RM), an industrial solid waste, has a huge gap between storage and utilization. Despite the global accumulation of over 4.6 billion tons of RM, its utilization rate remains only 4% [13]. This situation demonstrates the unsustainability of traditional disposal methods, which results in environmental pollution and resource wastage [14, 15]. RM is of great value and economically viable. It is rich in metal oxides (Fe_2O_3, Al_2O_3, SiO_2, and alkaline metals such as Na_2O, K_2O, and CaO), which makes it high reactivity in various chemical reactions [16, 17]. As the primary metal oxide in RM, Fe_2O_3 plays a crucial role in gasification by providing lattice oxygen to influence the reaction progression.

✉ Long Han
  longhan@zjut.edu.cn

1   Institute of Energy and Power Engineering, College of Mechanical Engineering, Zhejiang University of Technology, Chaowang Rd. 18, Hangzhou 310014, China

2   Quzhou Eco-Industrial Innovation Institute ZJUT, East Rongchang Rd. 2, Quzhou 324499, China

Consequently, utilizing RM as a potential oxygen carrier appears to be a promising choice in BCLG.

Many scholars have explored the utilization of iron-based oxygen carriers for solid fuel gasification [18–21]. For example, Huang et al. [20] observed that the presence of iron-based oxygen carriers significantly increased syngas yield compared to traditional steam gasification. Additionally, studies have revealed that reducing gases (e.g., H_2, CO, and CH_4) from gasification can easily react with oxygen carriers due to their good redox properties and gas–solid contact [17, 21–23]. Different iron-based oxygen carriers exhibit varying reactivity towards H_2 and CO produced during gasification. For example, Shen et al. [21] observed that the iron-based oxygen carrier reacted faster with H_2 than with CO and CH_4, leading to a decrease in gasification efficiency with increasing the content of the iron-based oxygen carrier. Rhodes et al. [24] and Hakkarainen et al. [25] indicated that iron-based oxygen carriers were active in the high-temperature water–gas shift reaction, converting CO produced from the tar into H_2 and CO_2. To date, the catalytic activity of RM has been studied in areas for methane reforming [26] and biomass oil upgrading [27, 28]. However, the use of RM as an oxygen carrier in BCLG remains limited [29]. Therefore, the feasibility of utilizing RM as a potential oxygen carrier in BCLG is still unknown.

It is well known that biomass-derived syngas from gasification contains unwanted tar due to the high volatile content of biomass [12]. Tar contains stubborn polycyclic aromatic hydrocarbons (PAHs) and other hydrocarbons that can adversely affect the composition and yield of syngas, as well as the operation of the equipment [30]. To date, iron oxides have been investigated as useful catalysts for tar decomposition, which could promote the breaking of C–C and C-H bonds within tar. Yang et al. [31] concluded that RM was effective for tar cracking at high temperature. Song et al. [32] found that the active Fe_2O_3 in RM was an important factor in the secondary cracking of pyrolytic tar. Although RM has demonstrated significant catalytic activity in tar conversion during pyrolysis [31, 32], there is limited literature available on the mechanism of RM in tar cracking during BCLG. So far only Cheng et al. [33] found that the RM realized the high conversion of tar model compound (naphthalene) in a wet syngas environment. During BCLG, the catalytic tar cracking process becomes more complex in the presence of steam, which participates in varying reactions such as tar reforming and water–gas shift reactions

[33]. More importantly, steam would alter the iron phase in RM, which could strongly affect the catalytic activity of RM for tar reduction. Fukase et al. [34] suggested that maintaining the reduced state of iron oxide during tar removal was desirable to prevent iron oxide deactivation. Matsuoka et al. [35] observed that Fe_3O_4 reduced from an iron-based catalyst could reform tar in the presence of steam. Recently, our research also revealed that the reduction and reoxidation reactions of the iron-based oxygen carrier in the steam atmosphere can reform the tar model compound to produce H_2 [36]. Overall, there has been limited research on the performance of RM on tar removal during the BCLG. To the best of the authors' knowledge, the performance of RM on syngas yield enhancement via tar reduction during BCLG has rarely been investigated. Therefore, it is interesting to clarify the chemical structure evolution of RM to detect the tar removal mechanism during the BCLG process.

This paper studied the BCLG process of corn cob as fuel with RM as an oxygen carrier. The effects of operating parameters, including O/C ratio, steam flow rate, and reaction temperature on the performance of BCLG were studied and optimized. The three-phase products after the reaction were analyzed, and the relationship between tar removal and syngas production was studied: Firstly, gasification performance was evaluated via collected information such as syngas yield, carbon conversion, and gasification efficiency; Secondly, the composition of collected tar was analyzed by GC–MS to study the catalytic performance of RM on tar removal; Ultimately, the raw RM and reaction residues were characterized through the H_2-TPR, XRD, and SEM to describe the main reduction pathways and surface morphologies of RM. These investigations are beneficial for optimizing the BCLG and mitigating the negative effect of tar in the BCLG.

2 Experimental

2.1 Materials

Corn cob as the fuel was obtained from Henan Province of China. The corn cob was sieved to 0.6–0.9 mm and then dried at 105 °C for 12 h. The proximate analysis and ultimate analysis of the corn cob are presented in Table 1.

The RM as the oxygen carrier was received from Henan Province of China. The RM was dried at 105 °C for 5 h to remove the free water. When cooled to room temperature,

Table 1 Proximate analysis and ultimate analysis of corn cob (wt. %, dried basis)

Sample	Proximate analysis				Ultimate analysis					$Q_{net,ad}$
	M_{ad}	A_{ad}	V_{ad}	FC_{ad}	C_{ad}	H_{ad}	N_{ad}	S_{ad}	O^*_{ad}	kJ/kg
Corn cob	10.95	6.41	67.31	15.33	44.21	4.75	0.51	0.60	32.57	15,670

M, moisture; *A*, ash; *V*, volatile; *FC*, fixed carbon; *ad*, air-dried basis. *By difference

Table 2 Elemental composition analysis of the RM (wt. %)

Component	Fe_2O_3	Al_2O_3	SiO_2	Na_2O	CaO	TiO_2	K_2O
Composition	27.74	25.50	20.01	11.09	8.18	3.99	1.21

Fig. 1 The schematic diagram of the fixed bed steam gasification experimental system
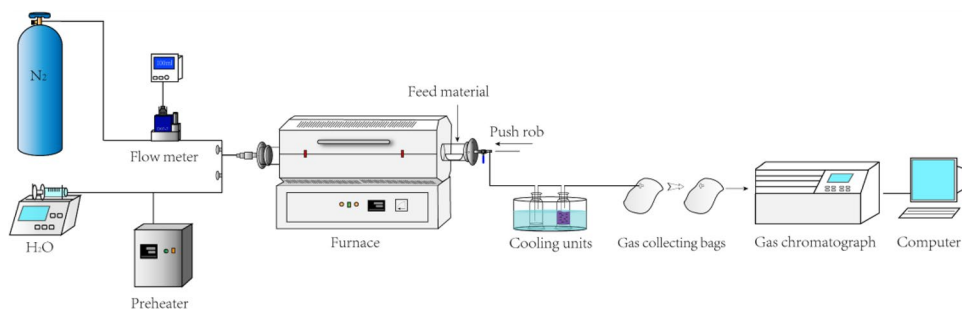
it was crushed and sieved to a particle size of 0.2–0.3 mm. Subsequently, these particles were calcined at 900 °C for 2 h in a muffle furnace to enhance their mechanical strength and remove impurities. The chemical compositions of the calcined RM were determined by X-ray fluorescence (XRF, ARL-9800, Switzerland), as shown in Table 2.

2.2 Experimental setup and procedure

The experimental system consisted of a gas supply unit, a horizontally fixed bed reactor, and a gas sampling and analyzing apparatus, as shown in Fig. 1. The reactor was a quartz tube with a total length of 1000 mm and an inner diameter of 45 mm. The gas supply unit provided mixed gases to the reactor, which consisted of 0.1 L/min N_2 controlled by a flowmeter and steam preheated from distilled water. Additionally, the unit included electric heating bands wrapped around the pipes to prevent steam condensation. When the reaction temperature reached the target, a crucible carrying a certain amount of RM and a total of 1 g corn cob was quickly pushed into the reaction zone to react rapidly for 13 min. The syngas from the reactor outlet was condensed, filtrated, and then sampled using a gas collection bag. After the completion of gasification, the feeding of steam and the heating of the external electrical furnace were stopped. Finally, the fixed bed reactor was gradually cooled down to room temperature at 0.1 L/min N_2. The specific operating conditions are summarized in Table 3 and the possible reactions in this gasification process that may occur are listed in Table 4.

The composition and concentration of the produced syngas were detected by a gas chromatograph-thermal conductivity detector (GC-TCD, Fuli GC-9790, China). N_2, H_2, CO, CO_2, and CH_4 were all detected. Tar was collected as described below: Firstly, the condensers and the connecting tubes were washed with dichloromethane; Secondly, the collected liquid was filtered and separated to remove impurities and water; Finally, the extracted organic phase was heated in a water bath at 45 °C to remove the dichloromethane. The

Table 3 Operating conditions used in the experimental campaign

Species	Operation parameters
Fuel and its mass	Corn cob (1 g)
Oxygen carrier	RM
Oxygen carrier mass	1.228 g, 2.456 g, 3.684 g, 4.912 g
Reaction temperature	700 °C, 750 °C, 800 °C, 850 °C
Inert gas and its flow rate	N_2 (0.1 L/min)
Steam agent flow rate	0 mL/min, 0.1 mL/min, 0.2 mL/min, 0.3 mL/min

collected tar was characterized by a gas chromatography-mass spectrometry (GC–MS, Agilent 6890-GCT Premier, Waters) equipped with an Agilent DB-5 MS chromatographic column (30 m × 0.25 mm × 0.25 μm). The spectra of chromatographic peaks were compared with the mass spectra in the NIST mass spectral database (NIST11) to identify the compounds present in the tar. Qualitative analyses of the tar components were performed based on the peak areas. The solid residue was removed from the reactor when the furnace cooled to room temperature. The crystalline phases and surface morphology of solid residues were evaluated by powder X-ray diffraction (XRD, PANalytical X'Pert PRO) and scanning electron microscopy (SEM, GT500), respectively. The iron phases in the oxygen carrier and their reducibility were determined by temperature-programmed reduction (TPR, AutoChem II 2920).

2.3 Data evaluation

The carbon conversion (X_c, %) is defined as the proportion of carbonaceous gases (CO, CH_4, and CO_2) to the carbon contained in solid fuels.

$$X_c = \frac{12 \times \int_0^t N_{\text{out}}\left(X_{CO} + X_{CH_4} + X_{CO_2}\right)dt}{22.4 \times m_{C,\text{fuel}}} \tag{1}$$

Table 4 The possible reaction that may occur during the experiment

Reactive properties	Reactions
Biomass pyrolysis	$Biomass \rightarrow char + tar + gases\left(H_2, CO, CO_2, and C_nH_m\right)$ (1)
Water–gas reaction	$C + H_2O \rightarrow CO + H_2$ (2)
	$C + 2H_2O \rightarrow CO_2 + 2H_2$ (3)
Boudouard reaction	$C + CO_2 \rightarrow 2CO$ (4)
Tar cracking	$Tar \rightarrow H_2 + CO + C_nH_m$ (5)
Water–gas-shift (WGS) reaction	$CO + H_2O \rightarrow CO_2 + H_2$ (6)
CO oxidation	$CO + 3Fe_2O_3 \rightarrow CO_2 + 2Fe_3O_4$ (7)
	$CO + Fe_3O_4 \rightarrow CO_2 + 3FeO$ (8)
	$CO + FeO \rightarrow CO_2 + Fe$ (9)
Partial oxidation of methane	$CH_4 + H_2O \rightarrow CO + 3H_2$ (10)
	$CH_4 + 12Fe_2O_3 \rightarrow 2H_2O + CO_2 + 8Fe_3O_4$ (11)
	$CH_4 + 4Fe_3O_4 \rightarrow 2H_2O + CO_2 + 12FeO$ (12)
	$CH_4 + 4FeO \rightarrow 2H_2O + CO_2 + 4Fe$ (13)
Iron-steam reaction	$H_2O + 3FeO \rightarrow H_2 + Fe_3O_4$ (14)
	$4H_2O + 3Fe \rightarrow 4H_2 + Fe_3O_4$ (15)
H_2 oxidation	$H_2 + 3Fe_2O_3 \rightarrow H_2O + 2Fe_3O_4$ (16)

where N_{out} is the gas volume flow at the reactor outlet; X_i is the relative volume fraction of produced gas; and $m_{c,fuel}$ is the mass of carbon contained in solid fuels.

The gas yield (G_v, m³/kg) is defined as the volume of produced syngas per kilogram of solid fuels, including H_2, CO, CO_2, and CH_4.

$$G_v = \frac{V_{out}\left(X_{CO} + X_{CH_4} + X_{CO_2} + X_{H_2}\right)}{m_{fuel}} \quad (2)$$

where V_{out} is the gas volume at the reactor outlet and m_{fuel} is the mass of solid fuels.

The lower heating value of the product syngas (LHV_{syngas}, MJ/m³) is defined as follows:

$$LHV_{syngas} = 10.798R_{H_2} + 12.636R_{CO} + 35.818R_{CH_4} \quad (3)$$

where R_i is the ratio of the volume of each gaseous component to the volume of produced gas in total.

The gasification efficiency (η, %) is defined as the ratio of LHV_{syngas} to the $LHV_{solid\,fuels}$.

$$\eta = \frac{G_v \cdot LHV_{syngas}}{LHV_{solid\,fuels}} \quad (4)$$

3 Results and discussions

3.1 Effects of oxygen/carbon (O/C) ratio

The O/C ratio in CLG plays a key role in controlling the lattice oxygen content delivered from the oxygen carrier to the fuel. In the fixed bed, the effect of the O/C ratio (0.25,

0.5, 1, and 2) in the BCLG was examined at a reaction temperature of 800 °C and a steam flow rate of 0.3 g/min, as shown in Fig. 2.

Figure 2(a) presents the gas yield of different gases (H_2, CO, CO_2, and CH_4) as a function of the O/C ratio. With an increase in the O/C ratio from 0.25 to 2, the yields of H_2 and CO_2 increased from 0.39 m³/kg and 0.09 m³/kg to 0.70 m³/kg and 0.18 m³/kg, respectively. The yield of CO initially increased from 0.26 m³/kg to 0.36 m³/kg, then decreased to 0.29 m³/kg. The CH_4 yield showed a relatively minor change but an overall downward trend. Biomass underwent thermal decomposition to produce gases and tar under the steam atmosphere (Reactions 1–4). In this process, the lattice oxygen in the RM provided the oxygen source for the gasification. Increasing the O/C ratio at the same amount of fuel means that the fuel received more lattice oxygen. Therefore, the partial oxidation reactions (Reactions 7–9 and 11–13) proceeded forward with the increase of the O/C ratio, resulting in the consumption of CO and CH_4. In other words, a higher O/C ratio promoted the full oxidation of carbon gases to CO_2 [22]. The H_2/CO ratio increased from 1.49 to 2.39 when the O/C ratio increased from 0.25 to 2, which differs from the gasification results by Luo et al. [23] and Huang et al. [37] using other iron-based oxygen carriers. The possible reason was that the RM played a dominant role in the tar cracking to increase gas yield (Reactions 5), compared to the oxidation of syngas by RM [38]. Correspondingly, the tar yield in Fig. 3 indicated that more carbon and hydrogen in tar could be converted into small-molecule gases. Moreover, a more important reason for the increased yields of H_2 and CO_2 was that the reduced RM might undergo iron-steam reactions where FeO and Fe were re-oxidized to Fe_3O_4 (Reactions 14 and 15) [39]. In addition,
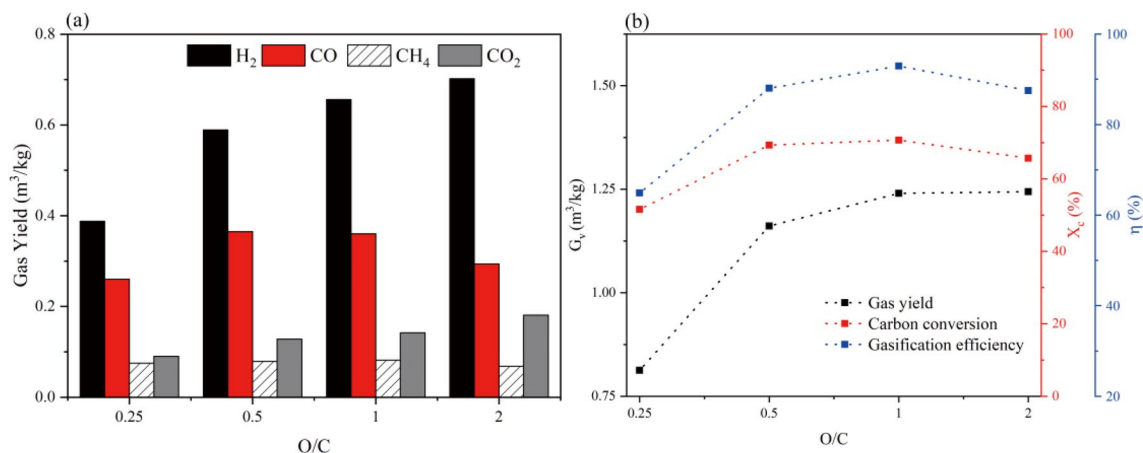
Fig. 2 The effect of the O/C ratio on (**a**) gas yield of different gases and (**b**) gas yield, carbon conversion efficiency, and gasification efficiency
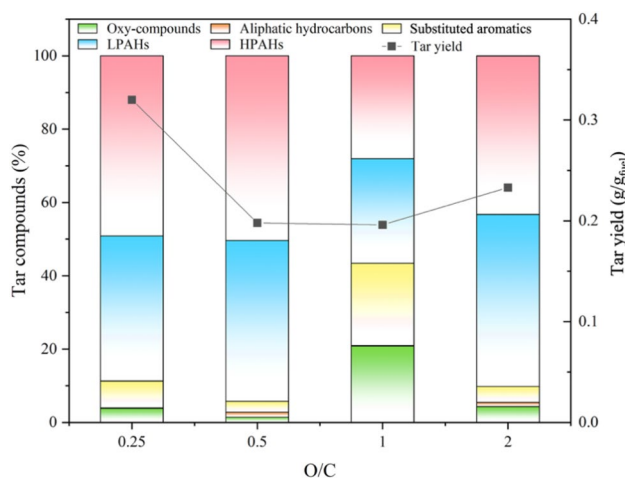

Fig. 3 Tar yield and components under different O/C ratio gasification

according to the XRD analyses, the iron phase in RM is primarily Fe_3O_4, which could provide sufficient active sites for the WGS reaction (Reactions 6) to enhance the yields of H_2 and CO_2 [29, 40, 41].

Figure 2(b) presents the gas yield, carbon conversion efficiency, and gasification efficiency as a function of the O/C ratio. With the O/C ratio increased from 0.25 to 2, gas yield, carbon conversion efficiency, and gasification efficiency increased by 0.43 m^3/kg, 14.14%, and 22.61%, respectively. The peak values of carbon conversion efficiency and gasification efficiency reached 70.74% and 92.95% at the O/C ratio of 1, respectively. Compared to natural iron ore [23] under similar gasification conditions, RM increased the gas yield, gasification efficiency, and carbon conversion efficiency by about 0.46 m^3/kg, 20%, and 25%, respectively. The gas yield and gasification efficiency are used to evaluate the reaction performance

[37]. It can be observed that gas yield was significantly increased with the increase of the O/C ratio. Although the gasification efficiency overall increased by 22.61%, it slightly decreased when the O/C ratio increased from 1 to 2. This was due to the fact that more combustible gases were converted to CO_2, which led to a decrease in LHV_{syngas}. There was no significant increase in gas yield and carbon conversion efficiency. Therefore, although increasing the content of the oxygen carrier could deliver more lattice oxygen to the fuel, the appropriate oxygen content was more favorable for carbon conversion efficiency and gasification efficiency. Based on the abovementioned results, an O/C ratio of 1 was suitable for achieving high-quality syngas in the BCLG.

Figure 3 presents the tar yield and its components as a function of the O/C ratio. With the O/C ratio increased from 0.25 to 2, the tar yield decreased significantly from 0.320 g/g_{fuel} to 0.233 g/g_{fuel}. The minimum tar yield reached 0.196 g/g_{fuel} at the O/C ratio of 1. Compared to manganese ore [38], RM exhibited excellent tar cracking ability in the BCLG, during which tar yield decreased by 38.75%. Increasing the O/C ratio facilitated the conversion of biomass tar to non-condensable gases, resulting in a lower tar yield. This matched the results for the gas-phase products. This may be due to the Fe_2O_3 and Al_2O_3 in RM reduced the tar yield by breaking C–C and C-H bonds in aromatic compounds [40, 42]. Meanwhile, the alkaline metals in RM could also catalyze tar cracking (Reaction 5) [43, 44], corresponding to the increase in H_2 yield observed in Fig. 2.

For a better understanding of the effect of RM on tar cracking during BCLG, the variations of tar components with the O/C ratio increase are shown in Fig. 3. Different from the single component of tar molds, biomass tar is a complex mixture that includes monocyclic aromatics, PAHs (including light PAHs (LPAHs, 2–3 rings) and heavy PAHs (HPAHs, 4–7 rings)), other benzene substituents, and a few

aliphatics [32]. Light tar species such as benzene and toluene were not observed due to their evaporative tendency during the collection and concentration [45]. To further analyze the changes in tar, the tar components detected by GC–MS were divided into five groups: (1) oxy-compounds, (2) aliphatic hydrocarbons, (3) substituted aromatics, (4) LPAHs, and (5) HPAHs. It can be observed that the relative content of HPAHs decreased as the O/C ratio increased in Fig. 3. In particular, there was a minimal relative content of LPAHs and HPAHs at the O/C ratio of 1, reaching 28.51% and 28.06%, respectively. Conversely, the content of oxy-compounds and substituted aromatics increased significantly to 20.88% and 22.42%, respectively. The aliphatic hydrocarbons were unaffected by the O/C ratio because aliphatic hydrocarbons were easily converted to stable aromatic hydrocarbons by Fe_2O_3 in RM at high temperature [46]. Furthermore, alkaline metals in RM accelerated the conversion of HPAHs to LPAHs [32, 33]. The O^{2-} ions in the active sites formed electron clouds with spatial diffusion that destabilized the π-electron clouds in tar, resulting in the cracking of HPAHs [47–49].

3.2 Effects of steam flow rate

Steam is reported as a good gasification agent to improve syngas and affect the flow field and heat-mass transfer in bed. In the fixed bed, the effect of the steam flow rate (0 g/min, 0.1 g/min, 0.2 g/min, and 0.3 g/min) in the BCLG was examined at an O/C ratio of 1 and a reaction temperature of 800 °C, as shown in Fig. 4.

Figure 4(a) presents the gas yield of different gases as a function of steam flow rate. With the steam flow rate increased, the yields of H_2 and CO_2 increased more than those of CO and CH_4. Notably, the H_2 yield increased significantly from 0.19 m^3/kg at pyrolysis to 0.52 m^3/kg at

the steam flow rate of 0.1 g/min, resulting in an increased H_2/CO ratio from 0.61 to 1.45. This result could be attributed to the promotion of the water–gas reaction (Reaction 2) by introducing steam. As the steam flow rate continued to increase, the yields of H_2 and CO_2 exhibited sustained growth. When the steam flow rate was 0.3 g/min, the maximum H_2 and CO_2 yield reached 0.66 m^3/kg and 0.14 m^3/kg, respectively. This indicated that a high concentration of steam further proceeded the water–gas reaction (Reaction 3) and the WGS reaction (Reaction 6). Moreover, steam played a role in promoting the iron-steam reactions (Reactions 14 and 15), which increased H_2 yield. The iron phase in RM was impacted by the presence of steam [20, 36]. Compared with Fig. 8, it was evident that the presence of FeO and Fe was observed in the absence of steam. This indicated that RM underwent significant reduction, which contributed to its sintering and agglomeration [50]. However, the reoxidation of the iron phase in RM by added steam inhibited the sintering and agglomeration of RM and produced more H_2. Additionally, controlling the CO/CO_2 ratio is essential for achieving high-quality syngas. With the addition of steam, the average CO yield was maintained at about 0.35 m^3/kg. The syngas quality was improved by introducing the mixture of steam and RM, as evidenced by the higher yield of CO than CO_2.

Figure 4(b) presents the gas yield, carbon conversion efficiency, and gasification efficiency as a function of the steam flow rate. All three parameters have a significant increase with increasing steam flow rate. When the steam flow rate increased from 0 to 0.3 g/min, the gas yield, carbon conversion efficiency, and gasification efficiency increased by 0.63 m^3/kg, 19.12%, and 39.40%, respectively. The addition of steam positively impacted gas yield and gasification efficiency, mainly due to the increased H_2 yield from the water–gas reactions. When the steam flow rate increased to
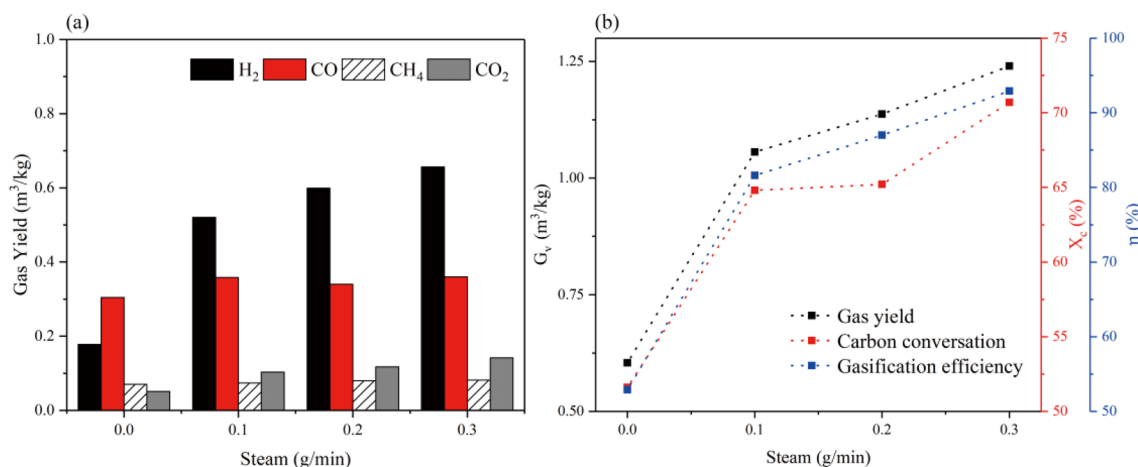

Fig. 4 The effect of steam flow rate on (**a**) gas yield of different gases and (**b**) gas yield, carbon conversion efficiency, and gasification efficiency

0.3 g/min, there was still potential to increase carbon conversion efficiency. It revealed that when more steam was introduced, more carbon in fuel was converted into syngas through carbon gasification reactions. Increasing the steam flow rate was beneficial for gasification reactions proceeding forward, which promoted fuel conversion more thoroughly. Besides, the tar reforming was accelerated by the higher steam flow rate, as shown in Fig. 5 [21]. Therefore, the steam flow rate was controlled at 0.3 g/min in subsequent work.

Figure 5 presents the tar yield and its components as a function of steam flow rate. With the steam flow rate increased from 0 to 0.3 g/min, the tar yield decreased significantly from 0.390 g/g_{fuel} to 0.196 g/g_{fuel}. The degree of tar cracking and conversion to gases in the presence of steam was more than the thermal decomposition in the pure N_2 atmosphere. The introduction of steam facilitated the tar reforming reaction (Reaction 5), which cracked the tar into small-molecular gases at 800 °C. As shown in Fig. 4, there was a significant increase in the gas yield, particularly in the H_2 yield. During the pyrolysis, the relative content of LPAHs in tar (53.81%) was higher than that of HPAHs (36.01%). XRD analysis revealed the gradual reduction of Fe_2O_3 in the RM to Fe that could efficiently break down the C–C and C-H bonds of aromatic hydrocarbons, thereby efficiently catalyzing tar cracking [51]. The tar composition showed a decrease in the relative content of HPAHs and an increase in the relative content of oxy-compounds, aliphatic hydrocarbons, substituted aromatics, and LPAHs with increasing steam flow rate. Compared to pyrolysis, the introduction of steam at 0.3 g/min steam flow rate resulted in a significant reduction of 33.25% in the relative content of PAHs. It can be attributed to the -O, -OH, and -H groups from the reforming gases, which promoted tar homogeneous conversion and inhibited PAHs formation [10]. On the one hand, the active -O free radical reacted with hydrocarbons to produce CO and H_2, as shown in Fig. 4. On the other hand, active -OH free radical inhibited the cyclization of aromatics by establishing a connection between the oxygen atom and hydrogen atom in hydrocarbons [52].

3.3 Effects of temperature

Numerous complex endothermic and exothermic reactions during the BCLG are involved, which are influenced by the reaction temperature. In the fixed bed, the effect of the reaction temperature (700 °C, 750 °C, 800 °C, and 850 °C) in the BCLG was examined at an O/C ratio of 1 and a steam flow rate of 0.3 g/min, as shown in Fig. 6.

Figure 6(a) presents the gas yield of different gases as a function of reaction temperature. It can be found that the overall trend in four gases increased with increasing temperature. With the temperature increased from 700 to 850 °C, the yields of H_2 and CO increased from 0.41 m^3/kg and 0.21 m^3/kg to 0.69 m^3/kg and 0.36 m^3/kg, respectively. On the contrary, the increase in CH_4 and CO_2 yield was limited from 0.07 m^3/kg and 0.1 m^3/kg to 0.08 m^3/kg and 0.16 m^3/kg. The variation in gas yield during the BCLG process results from a complex interplay between a series of competing reactions, gas/solid mixing, and fluid
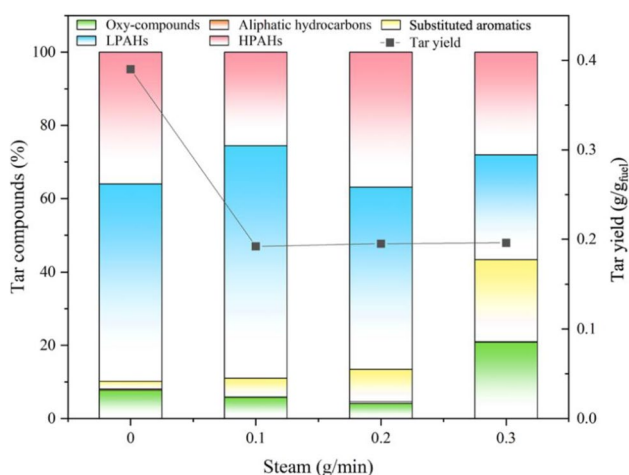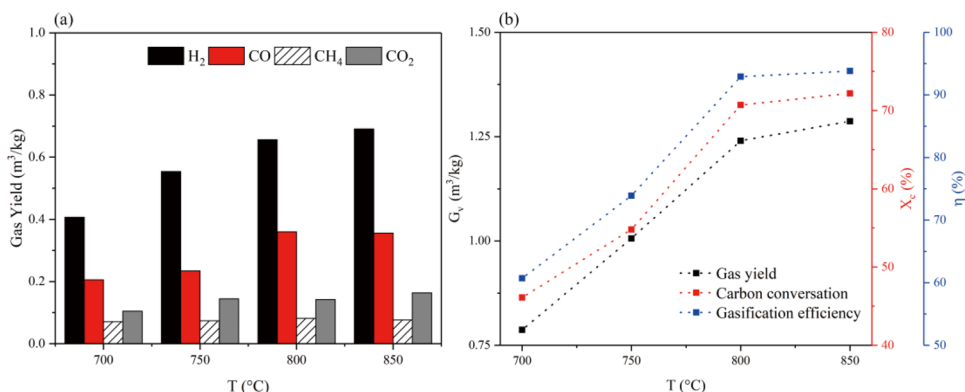

Fig. 5 Tar yield and components under different steam flow rate gasification

Fig. 6 The effect of temperature on (**a**) gas yield of different gases and (**b**) gas yield, carbon conversion efficiency, and gasification efficiency

dynamics [27]. The carbon and hydrogen in the fuel rapidly transformed into small-molecular gases under thermal conditions. High temperature significantly accelerated the biomass gasification process, resulting in more H_2 and CO yield in the fuel reactor. This result differs from the finding of Shen et al. [21] in BCLG using iron ore. The possible reason could be the different proportions of iron content in different iron-based oxygen carriers. At high temperature, oxygen carriers with higher iron oxide content are more likely to react with biomass-derived gases, resulting in rapid oxidation of H_2 and CO [21, 37]. The iron oxide content of RM (27.74%) is low compared to that of iron ore (83.21%). Therefore, although the oxidation reaction of oxygen carrier with syngas proceeded forward at high temperature (Reaction 7, 11, and 16), more intense gasification endothermic reactions such as water–gas reaction (Reaction 2, 3), tar cracking (Reaction 5), and methane reforming (Reaction 10) still resulted in the substantial increase in the yields of H_2 and CO. The yields of CO and CH_4 increased with the temperature rising to 800 °C and then slightly decreased with further temperature increase. This could be attributed to the CO oxidation reaction (Reaction 7) and the partial oxidation of methane reactions (Reactions 10 and 11). Simultaneously, the endothermic WGS reaction (Reaction 6) was promoted as the temperature increased from 800 °C to 850 °C, resulting in a slight increase in CO_2 yield.

Figure 6(b) presents the gas yield, carbon conversion efficiency, and gasification efficiency as a function of reaction temperature. All three parameters showed significant positive growth with the increase in temperature, which further reflected the sensitivity of gasification products to temperature variation. When the temperature increased from 700 to 850 °C, the gas yield, carbon conversion rate, and gasification efficiency increased by 0.50 m³/kg, 26.09%, and 33.10%, respectively. The initial increase in the three parameters below 800 °C was significant, indicating the increasing temperature enhanced primary pyrolysis in biomass and the reactivity of the condensable volatiles and solid products [11]. However, the growth of these parameters slowed down as the temperature increased from 800 to 850 °C, which is similar result by Luo et al. [23]. The reason for this was due to the low ash fusibility in corn cob, making it unable to withstand higher temperature. Additionally, the RM experienced agglomeration at high temperature, hindering its ability to catalyze further the gasification. Although increasing the reaction temperature could enhance the thermal reactions between the RM and biomass, it is essential to reasonably control the temperature in the BCLG to avoid high energy consumption and environmental pollution [53]. Therefore, a reaction temperature of 800 °C was determined as the optimal condition in this experiment.

Figure 7 presents the tar yield and its components as a function of reaction temperature. With the temperature increased from 700 to 850 °C, the tar yield decreased significantly from 0.36 g/g$_{fuel}$ to 0.187 g/g$_{fuel}$. Under the given material content and steam flow rate, the increase in gasification temperature substantially reduced tar yield. This result could be attributed to the relationship between temperature and rates of tar formation and cracking. Specifically, the tar cracking rate exceeded its formation rate during the temperature range of 700 to 800 °C, leading to a significant decrease in tar yield. This indicated that the process of tar cracking was more dominant during this temperature range. However, the decline in tar yield was not significant at temperature beyond 800 °C, suggesting that further temperature increases had a limited impact on tar cracking. Additionally, temperature significantly affected the tar components, particularly the HPAHs and other heterocyclic aromatic compounds. Increased temperature reduced heterocyclic aromatic compounds containing branching or heteroatom, such as pyridine, cresols, and quinoline [52, 54]. Compared to nonaromatic structures, aromatic ring structures possessed higher thermal stability. Consequently, PAHs tended to polymerize through dehydrogenation at high temperature, leading to an increase in their content. Overall, the temperature of 800 °C effectively cracked tar and converted PAHs into light tar species and non-condensable gases.

3.4 Characterization analyses of solid particles

Figure 8(a) presents the H_2-TPR curve of the raw RM, which depicts the variation in the valence of active components in raw RM with increasing temperature. Three consumption peaks of H_2 corresponded to different valences of iron
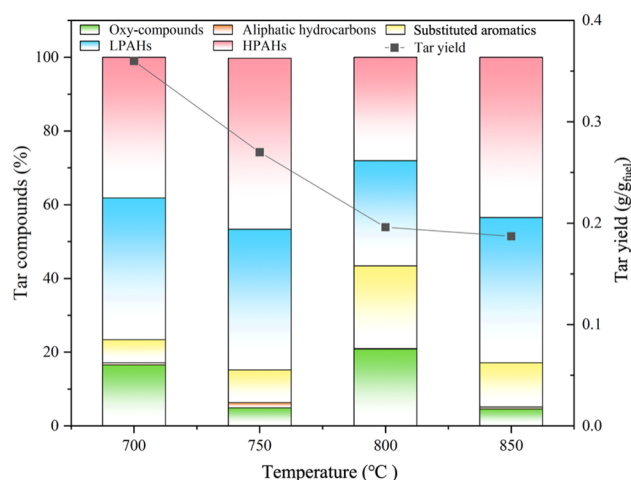

Fig. 7 Tar yield and components under different reaction temperature gasification

compounds in RM: Fe_2O_3—Fe_3O_4—FeO—Fe. Figure 8(b) presents the XRD patterns of the raw RM and the "corn cob & RM" residues after the pyrolysis and BCLG. The main active component in the raw RM was Fe_2O_3 and trace amounts of crystalline phases, including $CaTiO_3$, $NaAlSiO_4$, and $Ca_2Al_2SiO_7$. The iron phases in the RM during the reduction and reoxidation did not form new spinel phases by reacting with the support material. In addition, the Na and Ca elements in the RM interacted strongly with Al_2O_3 and SiO_2 during the thermal conversion process of pyrolysis and gasification [55]. Therefore, the peak values of $NaAlSiO_4$ and $Ca_2Al_2SiO_7$ were significantly increased compared to the raw RM. Figure 8(II) presents the presence of Fe and FeO in the "corn cob & RM" residue during the pyrolysis. The Fe_2O_3 in RM was deeply reduced into FeO and Fe without steam catalysis, indicating sufficient lattice oxygen was transferred from RM to fuel. Shen et al. [56] did not detect FeO or Fe during the pyrolysis, possibly because the chosen cyanobacteria tended to melt, which prevented interaction with RM. The result of BCLG with the steam flow rate of 0.3 g/min is presented in Fig. 8(III). Usually, iron-based oxygen carriers are gradually reduced due to the presence of large amounts of reducing gases. However, it was interesting to observe that the FeO and Fe did not exist when steam was added. This could be attributed to the reoxidation of FeO and Fe into Fe_3O_4, which was facilitated by adequate oxygen from the steam. The limitation of the deep reduction of RM by steam not only prevented its sintering but also produced more H_2, as discussed in Section 3.2. Overall, the iron phase reduction path of RM during BCLG can be described as Fe_2O_3—Fe_3O_4—FeO/Fe—Fe_3O_4.

Figure 9 presents the SEM images of the raw RM and the "corn cob & RM" residues after the pyrolysis and CLG. Compared to raw RM, the "corn cob & RM" residue after pyrolysis tended to agglomerate, but still retained a porous structure on the surface. This could be attributed to the inert components (Al_2O_3, SiO_2, and $NaAlSiO_4$) in RM that enhanced the sintering resistance. Compared to pyrolysis, the "corn cob & RM" residue in BCLG at the same

temperature exhibited a larger particle size but still retained a distinct pore structure. Adding steam effectively prevented the deep reduction of RM from alleviating its agglomeration and sintering based on XRD analysis. At the same steam flow rate, the residues at 750 °C and 800 °C exhibited different micro-pores. The residues at 750 °C maintained a well-defined surface structure with regular and abundant pores. However, when the reaction temperature was increased to 800 °C, the particle size significantly enlarged accompanied by agglomeration. This was related to the low ash fusibility of corn cob itself, and the presence of potassium elements in RM could also reduce the ash fusibility [57]. Therefore, the temperature in the BCLG process using RM as the oxygen carrier was recommended to be controlled at 800 °C.

4 Conclusions

In this paper, the performance of biomass chemical looping gasification (BCLG) was studied in a fixed bed reactor with industrial solid waste red mud (RM) as a novel oxygen carrier. The obtained results were expected to provide useful insights into using waste RM to enhance syngas quality and tar reduction during BCLG. The influence of RM on the evolution rules of gas-phase and liquid-phase products during gasification was analyzed under different key operational conditions (O/C ratio, steam flow rate, and temperature). Multiple characterization methods (XRF, XRD, H_2-TPR, and SEM) were applied to explore the primary components, iron phase reducibility, and surface structure of RM. The chemical characterization of RM was also adopted to detect the tar removal mechanism during BCLG.

RM exhibited good gasification performance as a potential oxygen carrier during BCLG. RM improved the gas yield and quality with a maximum H_2/CO ratio of 2.39 while reducing tar yield by 38.75%. With the increasing O/C ratio, heavy polyaromatic hydrocarbons (PAHs) were cracked into lighter tar species and non-condensable gases. Metal oxides

Fig. 8 a H_2-TPR profiles of raw RM catalysts. **b** The XRD patterns of the raw RM (I), the residues derived from the BCLG of 0 g/min (II) and 0.3 g/min (III) steam flow rate (reaction conditions: O/C = 1; gasification temperature 800 °C)
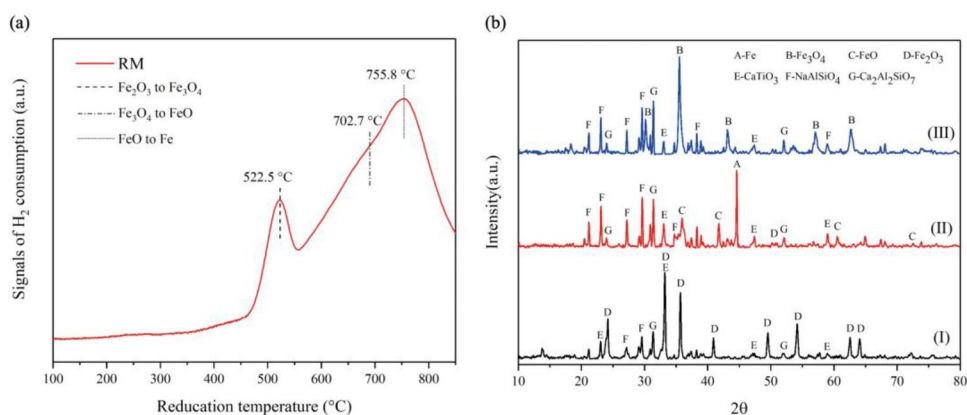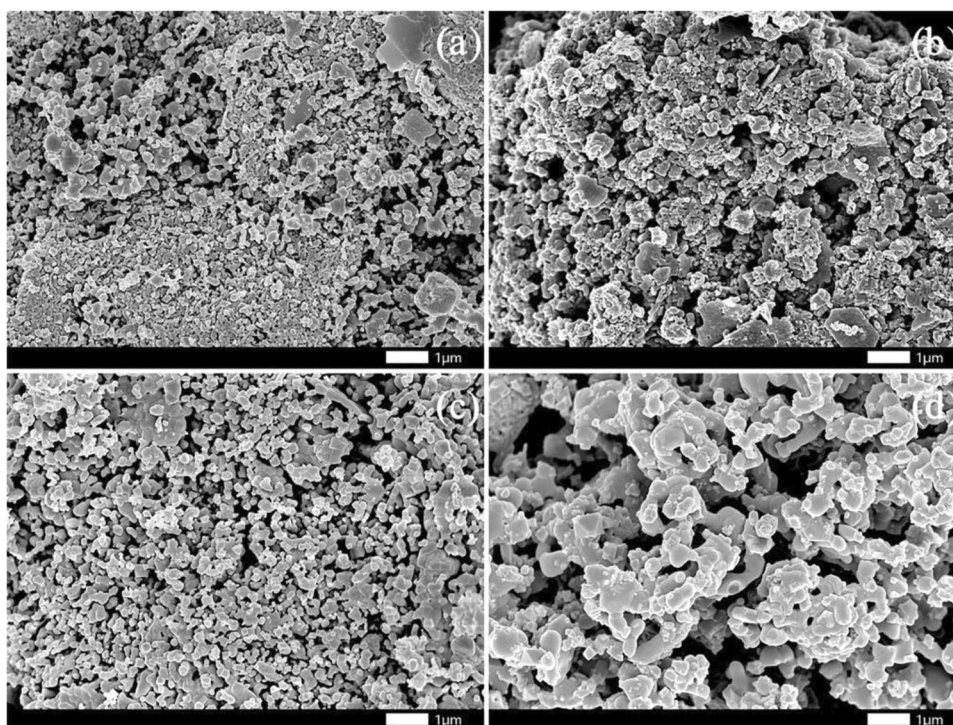
Fig. 9 SEM morphologies of raw RM and the residues derived from the BCLG. **a** Raw OC; **b** 0 g/min steam flow; **c** 750 °C; **d** 800 °C (reaction conditions: O/C = 1; steam flow rate 0.3 g/min)

within RM participated in reactions with steam. The limitation of intensive reduction of RM through iron-steam reactions not only prevented RM sintering but also enhanced hydrogen production. XRD analyses revealed the evolution of iron compounds in RM: Fe_2O_3—Fe_3O_4—FeO/Fe—Fe_3O_4. Furthermore, steam facilitated the tar homogeneous conversion and inhibited the formation of PAHs. The relative content of PAHs was significantly reduced by 33.25%. At the same O/C ratio and steam flow rate, increasing the reaction temperature facilitated endothermic reactions, resulting in the tar cracking into non-condensable gases. It was appropriate to control the temperature at 800 °C, because higher temperature would promote PAH polymerization via dehydrogenation. SEM analysis of "corn cob & RM" residues demonstrated no severe agglomeration and sintering of RM at 800 °C. Under the optimal conditions of BCLG (O/C ratio of 1, steam flow rate of 0.3 g/min, and reaction temperature of 800 °C), the carbon conversion efficiency, gasification efficiency, and gas yield reached 70.74%, 92.95%, and 1.24 m^3/kg, respectively. Meanwhile, the H_2/CO ratio reached 1.82, and the harmful tar was reduced to 0.196 g/g_{fuel} in BCLG.

Author contribution Conceptualization: Long Han and Zhonghui Wang; methodology: Zhonghui Wang and Jianhao Zhang; formal analyses and investigation: Zhonghui Wang and Zewei Shen; writing—original draft preparation: Zhonghui Wang and Yuelun Wu; writing—review and editing: Kaili Ma and Shengxiao Mao; funding acquisition: Long Han; resources: Long Han; supervision: Long Han.

Data Availability Not applicable.

Declarations

Ethical approval Not applicable.

Competing interests The authors declare no competing interests.

References

1. BP (2022) bp ENERGY OUTLOOK 2022. BP Publishing Web. https://ricn.sjtu.edu.cn/Kindeditor/Upload/file/20220315/202203151707001424332.pdf. Accessed 2022.
2. IPCC (2013) Climate Change 2013: The Physical Science Basis. Contribution of Working Group Ito the Fifth Assessment Report of the Intergovern mental Panel on Climate Change. Computational Geometry 1. https://doi.org/10.1016/S0925-7721(01)00003-7.
3. Zhao X, Zhou H, Sikarwar VS, Zhao M, Park A-HA, Fennell PS, Shen L, Fan L-S (2017) Biomass-based chemical looping technologies: the good, the bad and the future. Energy Environ Sci 10:1885–1910. https://doi.org/10.1039/c6ee03718f
4. Luo M, Yi Y, Wang S, Wang Z, Du M, Pan J, Wang Q (2018) Review of hydrogen production using chemical-looping technology. Renew Sustain Energy Rev 81:3186–3214. https://doi.org/10.1016/j.rser.2017.07.007

5. Wang P, Means N, Shekhawat D, Berry D, Massoudi M (2015) Chemical-Looping Combustion and Gasification of Coals and Oxygen Carrier Development: A Brief Review. Energies 8:10605–10635. https://doi.org/10.3390/en81010605

6. Lee M, Lim HS, Kim Y, Lee JW (2020) Enhancement of highly-concentrated hydrogen productivity in chemical looping steam methane reforming using Fe-substituted LaCoO₃. Energy Convers Manage 207:112507. https://doi.org/10.1016/j.enconman.2020.112507

7. Chen J, Zhao K, Zhao Z, He F, Huang Z, Wei G (2019) Identifying the roles of MFe_2O_4 (M=Cu, Ba, Ni, and Co) in the chemical looping reforming of char, pyrolysis gas and tar resulting from biomass pyrolysis. Int J Hydrogen Energy 44:4674–4687. https://doi.org/10.1016/j.ijhydene.2018.12.216

8. Abdalazeez A, Li T, Cao Y, Wang W, Abuelgasim S, Liu C (2022) Syngas production from chemical looping gasification of rice husk-derived biochar over iron-based oxygen carriers modified by different alkaline earth metals. Int J Hydrogen Energy 47:40881–40894. https://doi.org/10.1016/j.ijhydene.2022.09.185

9. Ge H, Guo W, Shen L, Song T, Xiao J (2016) Experimental investigation on biomass gasification using chemical looping in a batch reactor and a continuous dual reactor. Chem Eng J (Lausanne) 286:689–700. https://doi.org/10.1016/j.cej.2015.11.008

10. Qin T, Yuan S (2023) Research progress of catalysts for catalytic steam reforming of high temperature tar: A review. Fuel 331:125790. https://doi.org/10.1016/j.fuel.2022.125790

11. Zhang Y, Kajitani S, Ashizawa M, Oki Y (2010) Tar destruction and coke formation during rapid pyrolysis and gasification of biomass in a drop-tube furnace. Fuel 89:302–309. https://doi.org/10.1016/j.fuel.2009.08.045

12. Qin Y, Campen A, Wiltowski T, Feng J, Li W (2015) The influence of different chemical compositions in biomass on gasification tar formation. Biomass Bioenerg 83:77–84. https://doi.org/10.1016/j.biombioe.2015.09.001

13. Xue S, Wu Y, Li Y, Kong X, Zhu F, William H, Li X, Ye Y (2019) Industrial wastes applications for alkalinity regulation in bauxite residue: A comprehensive review. J Central South Univ 26:268–288. https://doi.org/10.1007/s11771-019-4000-3

14. Renforth P, Mayes WM, Jarvis AP, Burke IT, Manning DAC, Gruiz K (2012) Contaminant mobility and carbon sequestration downstream of the Ajka (Hungary) red mud spill: the effects of gypsum dosing. Sci Total Environ 421–422:253–259. https://doi.org/10.1016/j.scitotenv.2012.01.046

15. Zhu F, Liao J, Xue S, Hartley W, Zou Q, Wu H (2016) Evaluation of aggregate microstructures following natural regeneration in bauxite residue as characterized by synchrotron-based X-ray micro-computed tomography. Sci Total Environ 573:155–163. https://doi.org/10.1016/j.scitotenv.2016.08.108

16. Zhou X, Zhang L, Chen Q, Xiao X, Wang T, Cheng S, Li J (2023) Study on the mechanism and reaction characteristics of red-mud-catalyzed pyrolysis of corn stover. Fuel 338:127290. https://doi.org/10.1016/j.fuel.2022.127290

17. Zeng J, Xiao R, Zhang S, Zhang H, Zeng D, Qiu Y, Ma Z (2018) Identifying iron-based oxygen carrier reduction during biomass chemical looping gasification on a thermogravimetric fixed-bed reactor. Appl Energy 229:404–412. https://doi.org/10.1016/j.apenergy.2018.08.025

18. Wei G, Wang H, Zhao W, Huang Z, Yi Q, He F, Zhao K, Zheng A, Meng J, Deng Z, Chen J, Zhao Z, Li H (2019) Synthesis gas production from chemical looping gasification of lignite by using hematite as oxygen carrier. Energy Convers Manag 185:774–782. https://doi.org/10.1016/j.enconman.2019.01.096

19. Velasco-Sarria FJ, Forero CR, Adánez-Rubio I, Abad A, Adánez J (2018) Assessment of low-cost oxygen carrier in South-western Colombia, and its use in the in-situ gasification chemical looping combustion technology. Fuel 218:417–424. https://doi.org/10.1016/j.fuel.2017.11.078

20. Huang Z, Zhang Y, Fu J, Yu L, Chen M, Liu S, He F, Chen D, Wei G, Zhao K, Zheng A, Zhao Z, Li H (2016) Chemical looping gasification of biomass char using iron ore as an oxygen carrier. Int J Hydrogen Energy 41:17871–17883. https://doi.org/10.1016/j.ijhydene.2016.07.089

21. Ge H, Guo W, Shen L, Song T, Xiao J (2016) Biomass gasification using chemical looping in a 25 kW_th reactor with natural hematite as oxygen carrier. Chem Eng J (Lausanne) 286:174–183. https://doi.org/10.1016/j.cej.2015.10.092

22. Huang Z, He F, Feng Y, Liu R, Zhao K, Zheng A, Chang S, Zhao Z, Li H (2013) Characteristics of biomass gasification using chemical looping with iron ore as an oxygen carrier. Int J Hydrog Energy 38:14568–14575. https://doi.org/10.1016/j.ijhydene.2013.09.022

23. Luo M, Zhang H, Wang S, Cai J, Qin Y, Zhou L (2022) Syngas production by chemical looping co-gasification of rice husk and coal using an iron-based oxygen carrier. Fuel 309:122100. https://doi.org/10.1016/j.fuel.2021.122100

24. Rhodes C, Hutchings GJ, Ward AM (1995) Water-gas shift reaction: finding the mechanistic boundary. Catalysis Today 23:43–58. https://doi.org/10.1016/0920-5861(94)00135-O

25. Hakkarainen R, Salmi T, Keiski RL (2010) Comparison of the dynamics of the high-temperature water-gas shift reaction on oxide catalysts. Catal Today 20:395–408. https://doi.org/10.1002/chin.199502027

26. Song C, Li C, Zhu D, Chen W, Ai L, Huang N, Yang L, Guo C, Liu F (2023) Waste utilization of sewage sludge and red mud based on chemical looping catalytic oxidation. Fuel 332:125990. https://doi.org/10.1016/j.fuel.2022.125990

27. Karimi E, Briens C, Berruti F, Moloodi S, Tzanetakis T, Thomson MJ, Schlaf M (2010) Red mud as a catalyst for the upgrading of hemp-seed pyrolysis bio-oil. Energy Fuels 24:6586–6600. https://doi.org/10.1021/ef101154d

28. Saral JS, Ranganathan P (2022) Catalytic hydrothermal liquefaction of Spirulina platensis for biocrude production using Red mud. Biomass Convers Biorefinery 12:195–208. https://doi.org/10.1007/s13399-021-01447-4

29. Chen L, Yang L, Liu F, Nikolic HS, Fan Z, Liu K (2017) Evaluation of multi-functional iron-based carrier from bauxite residual for H_2-rich syngas production via chemical-looping gasification. Fuel Process Technol 156:185–194. https://doi.org/10.1016/j.fuproc.2016.10.030

30. Ren J, Liu Y, Zhao X, Cao J (2020) Biomass thermochemical conversion: a review on tar elimination from biomass catalytic gasification. J Energy Inst 93:1083–1098. https://doi.org/10.1016/j.joei.2019.10.003

31. Yang J, Xu X, Liang S, Guan R, Li H, Chen Y, Liu B, Song J, Yu W, Xiao K, Hou H, Hu J, Yao H, Xiao B (2018) Enhanced hydrogen production in catalytic pyrolysis of sewage sludge by red mud: thermogravimetric kinetic analysis and pyrolysis characteristics. Int J Hydrogen Energy 43:7795–7807. https://doi.org/10.1016/j.ijhydene.2018.03.018

32. Song J, Yang J, Liang S, Shi Y, Yu W, Li C, Xu X, Xiao J, Guan R, Ye N, Wu X, Hou H, Hu J, Xiao B (2016) Red mud enhanced hydrogen production from pyrolysis of deep-dewatered sludge cakes conditioned with Fenton's reagent and red mud. Int J Hydrogen Energy 41:16762–16771. https://doi.org/10.1016/j.ijhydene.2016.06.217

33. Cheng L, Wu Z, Zhang Z, Guo C, Ellis N, Bi X, Paul Watkinson A, Grace JR (2020) Tar elimination from biomass gasification syngas with bauxite residue derived catalysts and gasification char. Appl Energy 258:114088. https://doi.org/10.1016/j.apenergy.2019.114088

34. Fukase S, Suzuka T (1993) Residual oil cracking with generation of hydrogen: deactivation of iron oxide catalyst in the steam-iron reaction. Appl Catal A Gen 100:1–17. https://doi.org/10.1016/0926-860X(93)80111-3

35. Matsuoka K, Shimbori T, Kuramoto K, Hatano H, Suzuki Y (2006) Steam reforming of woody biomass in a fluidized bed of iron oxide-impregnated porous alumina. Energy Fuels 20:2727–2731. https://doi.org/10.1021/ef060301f

36. Ma K, Han L, Wu Y, Rong N, Xin C, Wang K, Ding H, Qi Z (2023) Synthesis of a composite Fe–CaO-based sorbent/catalyst by mechanical mixing for CO_2 capture and H_2 production: an examination on CaO carbonation and tar reforming performance. J Energy Inst 109:101256. https://doi.org/10.1016/j.joei.2023.101256

37. Huang Z, Xu G, Deng Z, Zhao K, He F, Chen D, Wei G, Zheng A, Zhao Z, Li H (2017) Investigation on gasification performance of sewage sludge using chemical looping gasification with iron ore oxygen carrier. Int J Hydrogen Energy 42:25474–25491. https://doi.org/10.1016/j.ijhydene.2017.08.133

38. Wang S, Song T, Yin S, Hartge EU, Dymala T, Shen L, Heinrich S, Werther J (2020) Syngas, tar and char behavior in chemical looping gasification of sawdust pellet in fluidized bed. Fuel 270:117464. https://doi.org/10.1016/j.fuel.2020.117464

39. Vovk I, Melekhov R (1996) Role of iron oxide deposits in corrosion damage to the surfaces of steam-generating tubes of boilers of thermal power plants. Mater Sci 31:127–130. https://doi.org/10.1007/BF00565986

40. Azharuddin M, Tsuda H, Wu S, Sasaoka E (2008) Catalytic decomposition of biomass tars with iron oxide catalysts. Fuel 87:451–459. https://doi.org/10.1016/j.fuel.2007.06.021

41. Virginie M, Adánez J, Courson C, de Diego LF, García-Labiano F, Niznansky D, Kiennemann A, Gayán P, Abad A (2012) Effect of Fe–olivine on the tar content during biomass gasification in a dual fluidized bed. Appl Catal B 121–122:214–222. https://doi.org/10.1016/j.apcatb.2012.04.005

42. Zhao H, Li Y, Song Q, Lv J, Shu Y, Liang X, Shu X (2016) Effects of iron ores on the pyrolysis characteristics of a low-rank bituminous coal. Energy Fuels 30:3831–3839. https://doi.org/10.1021/acs.energyfuels.6b00061

43. Xu G, Murakami T, Suda T, Matsuzawa Y, Hidehisa T, Mito Y (2008) Enhanced conversion of cellulosic process residue into middle caloric fuel gas with Ca impregnation in fuel drying. Energy Fuels 22:3471–3478. https://doi.org/10.1021/ef800073w

44. Boroson ML, Howard JB, Longwell JP, Peters WA (1989) Heterogeneous cracking of wood pyrolysis tars over fresh wood char surfaces. Energy Fuels 3:735–740. https://doi.org/10.1021/ef00018a014

45. Wang J, Zhang S, Xu D, Zhang H (2022) Catalytic activity evaluation and deactivation progress of red mud/carbonaceous catalyst for efficient biomass gasification tar cracking. Fuel 323:124278. https://doi.org/10.1016/j.fuel.2022.124278

46. Jin Q, Wang X, Li S, Mikulčić H, Bešenić T, Deng S, Vujanović M, Tan H, Kumfer BM (2019) Synergistic effects during co-pyrolysis of biomass and plastic: Gas, tar, soot, char products and thermogravimetric study. J Energy Inst 92:108–117. https://doi.org/10.1016/j.joei.2017.11.001

47. Zhu T, Zhang S, Huang J, Wang Y (2000) Effect of calcium oxide on pyrolysis of coal in a fluidized bed. Fuel Process Technol 64:271–284. https://doi.org/10.1016/s0378-3820(00)00075-8

48. Han L, Wang Q, Yang Y, Yu C, Fang M, Luo Z (2011) TG-FTIR study on pyrolysis of wheat-straw with abundant CaO additives. Spectrosc Spectr Anal 31:942–946. https://doi.org/10.3964/j.issn.1000-0593(2011)04-0942-05

49. Jia Y, Huang J, Wang Y (2004) Effects of calcium oxide on the cracking of coal tar in the freeboard of a fluidized bed. Energy Fuels 18:1625–1632. https://doi.org/10.1021/ef034077v

50. Mendiara T, Abad A, de Diego LF, Garcia-Labiano F, Gayan P, Adanez J (2012) Use of an Fe-Based residue from alumina production as an oxygen carrier in chemical-looping combustion. Energy Fuel 26:1420. https://doi.org/10.1021/ef201458v

51. Nordgreen T, Liliedahl T, Sjostrom K (2006) Metallic iron as a tar breakdown catalyst related to atmospheric, fluidised bed gasification of biomass. Fuel 85:689–694. https://doi.org/10.1016/j.fuel.2005.08.026

52. Feng D, Zhao Y, Zhang Y, Sun S (2017) Effects of H_2O and CO_2 on the homogeneous conversion and heterogeneous reforming of biomass tar over biochar. Int J Hydrogen Energy 42:13070–13084. https://doi.org/10.1016/j.ijhydene.2017.04.018

53. Shen X, Yan F, Zhang Z, Li C, Zhao S, Zhang Z (2021) Enhanced and environment-friendly chemical looping gasification of crop straw using red mud as a sinter-resistant oxygen carrier. Waste Manage 121:354–364. https://doi.org/10.1016/j.wasman.2020.12.028

54. Han J, Kim H (2008) The reduction and control technology of tar during biomass gasification/pyrolysis: An overview. Renew Sustain Energy Rev 12:397–416. https://doi.org/10.1016/j.rser.2006.07.015

55. Fan Y, Zhang H, Lyu Q, Zhu Z (2020) Investigation of slagging characteristics and anti-slagging applications for Indonesian coal gasification. Fuel 267:117285. https://doi.org/10.1016/j.fuel.2020.117285

56. Zhang H, Chen L, Liu X, Ge H, Song T, Shen L (2021) Characteristics of cyanobacteria pyrolysis and gasification during chemical looping process with red mud oxygen carrier. J Fuel Chem Technol 49:1802–1810. https://doi.org/10.1016/s1872-5813(21)60087-7

57. Ding L, Zhang Y, Wang Z, Huang J, Fang Y (2014) Interaction and its induced inhibiting or synergistic effects during co-gasification of coal char and biomass char. Bioresour Technol 173:11–20. https://doi.org/10.1016/j.biortech.2014.09.007